Nanometer Scale Mechanical Properties of Au(111) Thin Films

M. Salmeron,* A. Folch,† G. Neubauer,‡ M. Tomitori,§ and D. F. Ogletree

Materials Science Division, Center for Advanced Materials, Lawrence Berkeley Laboratory, Berkeley, California 94720

W. Kolbe

Engineering Division, Lawrence Berkeley Laboratory, Berkeley, California 94720

Received March 20, 1992. In Final Form: July 22, 1992

The mechanical properties of gold films of (111) orientation were studied as a function of load when contacted by a single asperity Pt-Rh alloy tip. The interaction forces were measured in the direction perpendicular to the surface. The contribution of various types of forces (van der Waals, capillarity from contaminants, and metallic adhesion) in the process of contact was determined. We investigated the elastic and plastic response of the gold film as a function of applied load by examination of the contact area in subsequent imaging with STM and AFM.

1. Introduction

The advent of the scanning tunneling microscope (STM) and the atomic force microscope (AFM) has opened the way for studies of the mechanical properties of surfaces at the atomic scale. The number of recent publications in this area[1-7] indicates the potential of these modern techniques. Perhaps the most significant aspect of these techniques is their inherent capability to approximate the ideal single asperity contact that is used in all basic models of contact and adhesion.[8] The surface can be imaged with nanometer resolution using the same asperity so that the effect of contacts on the surface morphology can be ascertained. This permits us to distinguish the regimes of elastic and plastic deformation. Small forces can be applied to produce indentations only a few layers deep. Since the contact area is only a few nanometers, dislocations in the perfect crystal may not be generated since for small loop lengths the energy required is very high compared to the energy required to create point defects. Size effects may also play an important role since the area of contact is much smaller than the dimensions of the gold crystallites.

Similar techniques can be used to investigate the effect of adsorbates on asperity contacts. This relates closely to basic studies of lubrication. In a forthcoming paper we will discuss the properties of Au(111) films covered with self-assembled alkanethiol monolayers.

AFM experiments in ambient conditions always involve uncertainties in the surface composition. Contaminants modify the forces and currents between tip and surface. This is particularly true a few nanometers before and immediately after contact. However, as we will see, these effects can be separated. We show that in spite of this less controlled environment, a substantial amount of information can be gained on the mechanical properties of the gold substrate, particularly when the force becomes repulsive after contact, and during the transition between elastic and plastic regimes. When large forces are applied, the effect of contaminants is relatively unimportant. In most practical situations, friction and adhesion take place in air and the effect of contaminants is always present. AFM experiments are now in progress in our laboratory that will extend the present work to interfaces in ultrahigh vacuum environments.

2. Experimental Section

2.1. The AFM Instrument. The experiments were conducted with an AFM that uses interferometry to measure the displacement of the cantilever tip. The design is similar to that of Erlandsson et al.[9] except for the sample scanner. This was built from two piezoelectric tubes of 0.85 and 0.50 in. o.d. and 1 in. length mounted concentrically. The cantilever is attached to the edge of the outer tube by magnetic clamping. A small piezoelectric slab attached to the magnet can oscillate the cantilever for ac measurements. The sample is mounted on a small holder that rides on quartz rails glued to the inside walls of the inner piezo tube. This tube is expanded and contracted with an asymmetric voltage waveform that moves the sample toward the cantilever by inertial displacement.[10] Once in range, voltages are applied to this piezo tube to scan the sample under the tip. A single mode optical fiber of 4 μm core diameter is brought within a few micrometers of the back of the cantilever. This gap forms the interference cavity. To maintain gap stability against thermal drift and low frequency noise, the fiber is

† Permanent address: Departament de Física, Universitat de Barcelona, Barcelona, Spain.

‡ Present address: Intel Corporation, 2200 Mission College Blvd., Santa Clara, CA 95052.

§ Department of Materials Science and Engineering, Tokyo Institute of Technology, Yokohama 227, Japan.

(1) Mate, C. M.; McClelland, G. M.; Erlandsson, R.; Chiang, S. *Phys. Rev. Lett.* **1987**, *59*, 1942.

(2) Kaneko, R.; Nonaka, K.; Yasuda, K. *J. Vac. Sci. Technol.* **1988**, *A6*, 291.

(3) Miller, R. G.; Briant, P. J. *J. Vac. Sci. Technol.* **1989**, *A7*, 2879.

(4) Burnham, N. A.; Dominguez, D. D.; Mowery, R. L.; Colton, R. J. *Phys. Rev. Lett.* **1990**, *64*, 1931.

(5) Burnham, N. A.; Colton, R. J. *J. Vac. Sci. Technol.* **1989**, *A7*, 2906.

(6) Cohen, S. R.; Neubauer, G.; McClelland, G. M. *J. Vac. Sci. Technol.* **1990**, *A8*, 3449.

(7) Heinzelmann, H.; Meyer, E.; Rudin, H.; Güntherodt, H. J. *Scanning Tunneling Microscopy and Related Methods*, NATO ASI Series; Behm, R. J., Garcia, N., Rohrer, H., Eds.; Kluwer Academic Press. Dordrecht, The Netherlands, 1989; pp 443-469.

(8) For a review see the classical book: Bowden, F. P.; Tabor, D. *The Friction and Lubrication of Solids*; Oxford University Press, Part I, Clarendon Press: Oxford, 1950.

(9) (a) Erlandsson, R.; Hadziioannou, G.; Mate, C. M.; McClelland, G. M.; Chiang, S. *J. Vac. Sci. Technol.* **1988**, *A6*, 266. (b) Rugar, D.; Mamin, H. J.; Erlandsson, R.; Stern, J. E.; Terris, B. D. *Rev. Sci. Instrum.* **1988**, *59*, 2337.

(10) (a) Lyding, J. W.; Skala, S.; Brockenbrough, R.; Hubacek, J. S.; Gammie, G. *J. Microsc.* **1988**, *152*, 371. (b) Zeglinski, D. M.; Ogletree, D. F.; Beebe, T. P.; Hwang, R. Q.; Somorjai, G. A.; Salmeron, M. *Rev. Sci. Instrum.* **1990**, *61*, 3769.

0743-7463/92/2408-2832$03.00/0

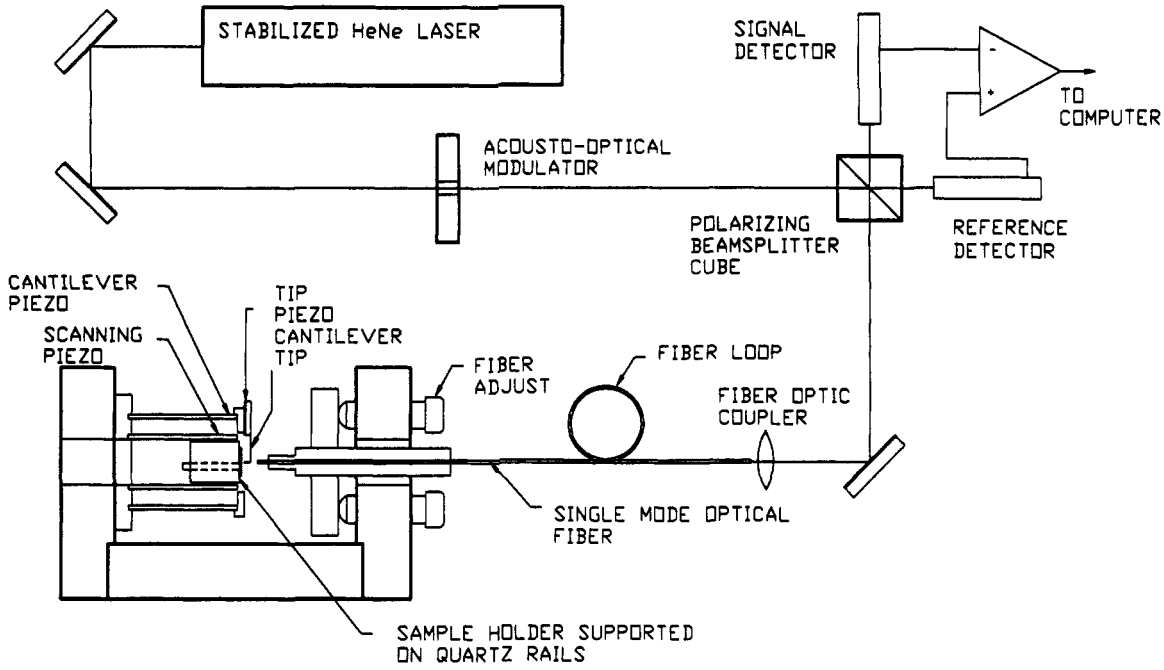

Figure 1. Schematic drawing of the combined STM/AFM apparatus used in this work. A He–Ne laser beam is transported by a fiber optic and reflected from the back of the cantilever tip. The gap between the fiber optic end and the cantilever wire is the interference cavity used to measure the gap distance. The interference signal is measured at the signal detector photodiode. The sample is mounted on two quartz rails glued to the inside walls of a tube piezoelectric that serves to translate the sample inertially toward the tip and then to scan for imaging and approach experiments. A small piezo supports the cantilever and is used to oscillate it in the direction perpendicular to the sample.

supported by a piezoelectric tube whose length is adjusted by a slow feedback circuitry that keeps the interferometer signal constant with time. Figure 1 shows a schematic of the experimental set up.

2.2. Tips. The tips used in the experiments were prepared from 75 and 127 μm diameter Pt–Rh(13%) alloy wires. Their length was typically 2–4 mm and they were bent in an L shape. The end of the short arm of the L was etched electrochemically in a molten salt solution of 80% $NaNO_3$ and 20% NaCl. By application of a bias of +2 V, the tip was sharpened to a radius of around 0.1 μm, as determined by scanning electron microscopy. The tips were spot welded to a gold-plated iron bar mounted on a small permanent magnet attached to the edge of the external piezo tube. The mechanical resonance frequency of these cantilevers f, varied between 4 and 7 kHz. The Q factor was typically 20–50. The spring constant k varied between 120 and 320 N/m.

The gold samples were produced by evaporation onto a mica or silicon wafer substrate.[11] When observed in the STM, the films showed large flat terraces and monoatomic steps, characteristic of the (111) orientation. Atomically resolved images showed the hexagonal lattice of Au(111). On silicon, the gold crystallites were smaller than on the mica substrate but exposed many flat surfaces also characterstic of the (111) orientation.

2.3. Modes of Operation. Two basic types of experiments were performed. In the first type, a physical parameter, P (P = lever deflection δ, oscillation amplitude A, tunneling current I), is measured as a function of sample displacement distance toward the tip, d. This distance is measured from the initial position of the sample, typically a few hundred angstroms away from the tip. The plots of P versus d are referred to as approach curves (APC's). Any two of these parameters could be measured simultaneously in an APC. The data acquisition time for a typical APC was 0.2 s.

The displacement d must not be confused with the tip-to-sample separation s. The distance s can be obtained from d and δ by substraction: $s = d - d_0 - \delta$. The distance d_0 being defined by the intersection of the extrapolated asymptotic line from the repulsive part of the force curve (see broken lines in Figure 2). This method of obtaining s, however, is only valid for infinitely rigid materials. For real materials, d_0 represents the position of the surface after deformation by the applied force and is different from the position before the application of the load. For this reason we prefer to display the APC data as a function of d since this is measured directly.

The lever deflection δ is proportional to the force exerted by the tip on the sample. This force F is obtained from δ by multiplication by the spring constant: $F = k\delta$.

The free resonance frequency of a cantilever is modified by the tip–surface interaction potential, as shown in the elegant experiments of Dürig et al.[12] This effect can be used to measure and map force gradients on the surface. In our experiments, the cantilever was oscillated by modulating the voltage applied to a supporting piezo slab near resonance. The modulated light intensity from the cavity, referred to as lever deflection signal, was measured at the photodetector (see Figure 1) and fed into a lock-in amplifier. The phase of the lock-in amplifier was adjusted to maximize the signal when the lever was far away from the surface. We refer to this as the *in-phase* amplitude A. Near resonance, as the tip interacts with the surface, the phase and amplitude change. For any oscillator, the time constant of this change depends on the ratio Q/f, which in our case is typically 5 ms. Therefore, any interaction that changes the force constant of the combined cantilever–surface system, will produce large and rapid changes in A.[13,14] This parameter is thus very sensitive to the presence of forces near the surface, like those arising from van der Waals interactions, or from the presence of weakly bound contaminants.

In the second type of experiments, the surface is imaged under feedback control. The control parameter was the tunnel current I, for the STM mode, or the cantilever in-phase amplitude A, for the AFM ac mode, sometimes called also the attractive mode. In the AFM ac mode the attractive force gradient above the surface shifts the cantilever resonance frequency and produces a change in A that is very sensitive to the distance. Occasionally the repulsive force measured by the deflection of the tip, δ, was used

(11) The gold on silicon samples were kindly prepared by C.E.D. Chidsey, AT&T Bell Labs, Murray Hill, NJ.

(12) Dürig, U.; Gimzewski, J. K.; Phol, D. W. *Phys. Rev. Lett.* **1986**, *57*, 2403.

(13) Marti, O.; Drake, B.; Hansma, P. K. *Appl. Phys. Lett.* **1987**, *51*, 484.

(14) Erlandsson, R.; McClelland, G. M.; Mate, C. M.; Chiang, S. *J. Vac. Sci. Technol.* **1988**, *A6*, 266.

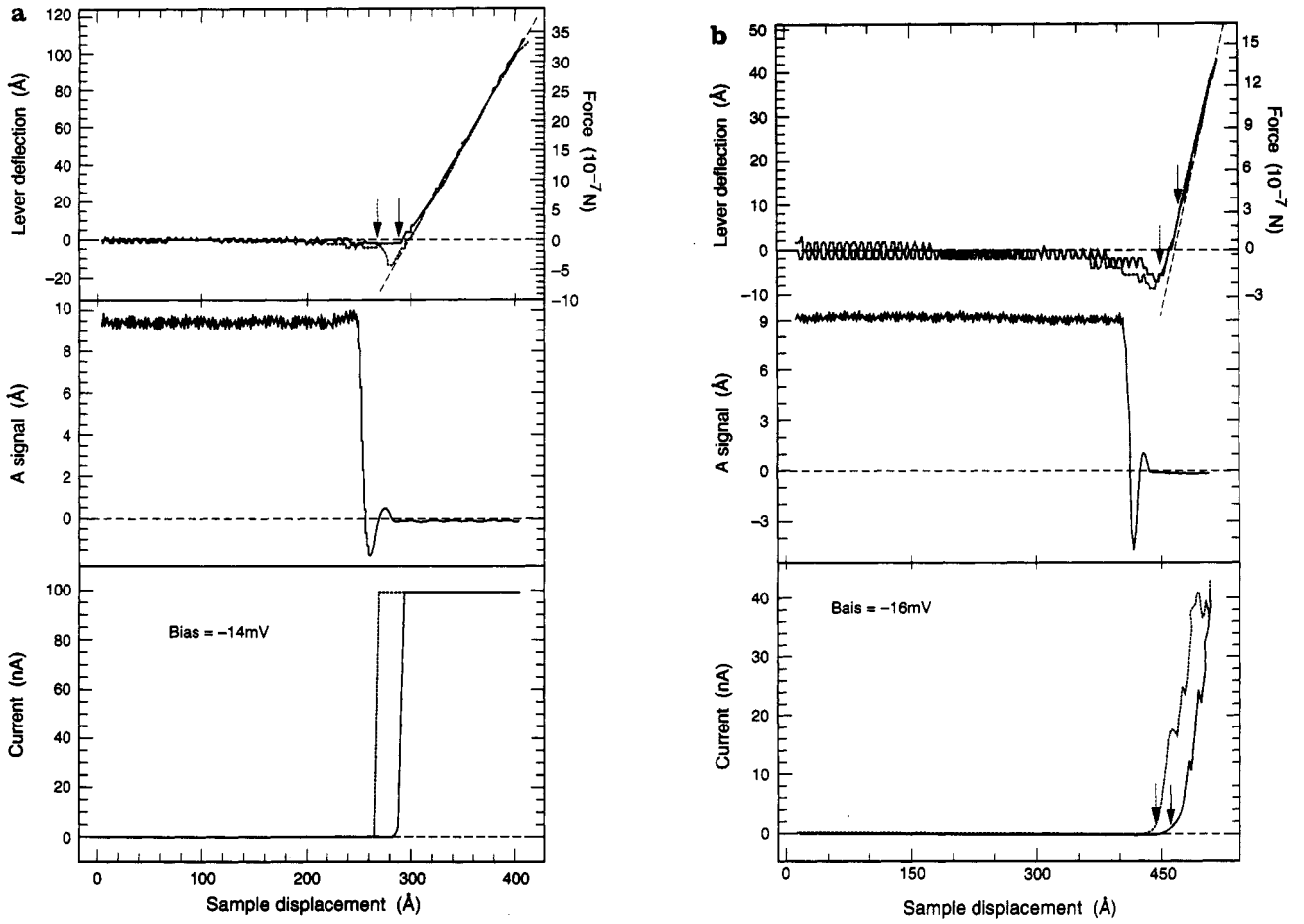

Figure 2. Sets of approach curves showing the lever deflection or force versus sample displacement toward the tip (top curves). Continuous curves represent sample displacement toward the tip while broken curves represent the reverse displacement away from the tip. The middle curves represent the in-phase oscillation amplitude of the cantilever, near its resonance frequency (4–7 kHz). This amplitude is very sensitive to forces and decays rather bruptly at a distance of 20–40 Å from the point of zero net force. The bottom curves represent the tunnel current for a small sample bias voltage. The two sets (a and b) represent two common types of contacts. In (a), the clean type, the current grows very rapidly, reaching several nA before contact (see arrows in the top curves). In (b), a contaminated contact, a repulsive force is needed to observe tunnel current, as shown by the arrows at the 1-nA current point.

as the control parameter (dc mode or contact mode of AFM imaging). Since our data acquisition software[15] can collect an auxiliary signal in addition to the controlling signal, the following combinations of control and auxiliary parameters were used in different imaging experiments: (1) STM (I = control) + lever deflection (or dc force); (2) STM (I = control) + amplitude A (or ac-force); (3) ac AFM (A = control) + current I; (4) dc AFM (lever deflection δ = control).

3. Results

3.1. Approach Curves. Influence of Contaminants. Figure 2 shows two sets of APC's representative of two main types of contacts we encountered. The top curves in each set correspond to the lever deflection, which is converted to force F by multiplying by the spring constant. The middle curves correspond to the cantilever in-phase oscillation amplitude A during approach. Finally, the bottom curves correspond to the tunnel current I, for a bias of about −15 mV applied to the sample. These sets of curves are composites of two consecutive APC's, one recording δ and A the other δ and I. In all cases, at separations greater than 50 Å from the point of zero net force (where the top curves in the figure cross the x-axis), the force is smaller than the noise level of $\approx 5 \times 10^{-9}$ N. At approximately 20–40 Å the lever deflects toward the sample, indicating a net attractive force. A minimum is then reached with an absolute value F_m^i, during approch, that can differ substantially from the minimum F_m^o observed upon retraction (broken line curves). As we shall see, the value of F_m^o is a function of the maximum applied force or load F_M. The value of F_m^i on the other hand was found to vary between different experiments as a result, we believe, of the contamination present. We address this point in the next section.

3.1.1. Types of Contacts. The various types of contacts observed are distinguished by the magnitude of the force minimum F_m^i and by the onset position and rate of increase of the tunnel current I. For simplicity and convenience, we classify them into two broad categories. The first category (type I), includes contacts characterized by APC's such as those shown in Figure 2a: I (bottom curves) increases very rapidly in a few angstroms of sample displacement, the increase taking place at or before the minimum of F is reached (the arrows in the figure mark the point where I reaches 1 nA). Another example of contacts in this category is shown in Figure 3 where I increases rapidly to saturate the preamplifier at 10 nA a few angstroms *before* reaching the minimum of F. The value of F_m^i is usually between (0.1 and 1.5) $\times 10^{-7}$ N in these types of contacts while that of F_m^o is *always* larger. This is true even when the force applied by the cantilever at the closest approach F_M, is negative (attractive), as in Figure 3.

(15) Developed by D. F. Ogletree, licensed to RHK Technology, Rochester Hills, MI 48309.

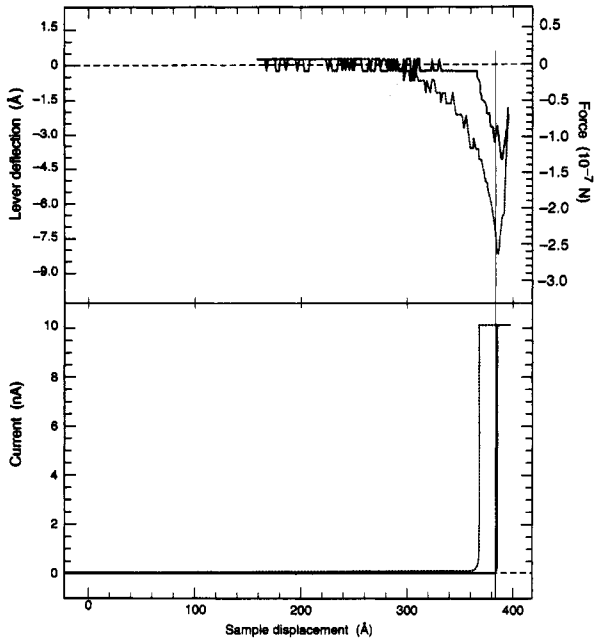

Figure 3. Expanded approach curve showing the force curve (top) during approach and the current I (bottom) for a type I contact. The continuous line corresponds to sample displacement toward the tip while the broken one corresponds to the reverse displacement away from the tip. Notice the rapid increase of I that exceeds 10 nA at approximately 7 Å from the minimum of F. Sample bias $V = -13$ mV.

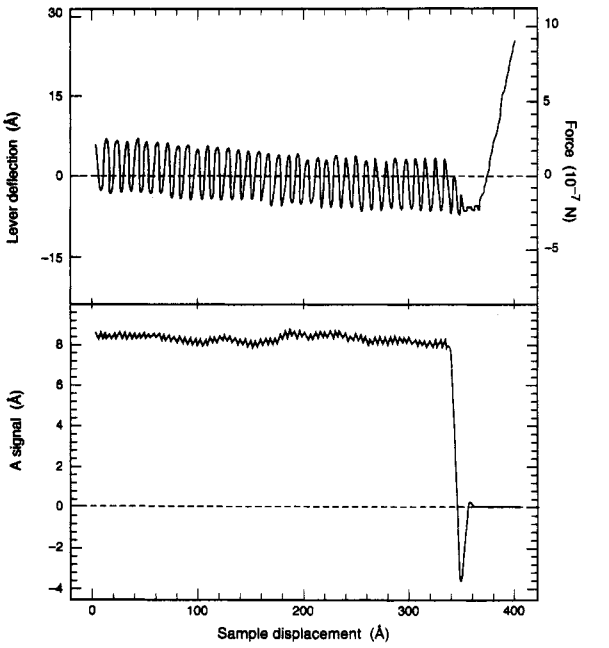

Figure 4. Force curve during an approach experiment with an oscillating cantilever. The amplitude A is 9 Å peak-to-peak at near resonance. The frequency in this graph appears lower than the real frequency (about 5 kHz) due to the smaller data collection frequency (1 kHz). Notice the decay of A in the attractive force region and the value of near zero reached at the minimum. The in-phase signal as given by a lock-in amplifier is shown at the bottom. Notice the negative excursion due to a phase change past 90°. A 50% reduction in the signal is reached 20 Å before the minimum of F.

The second category (type II) includes contacts characterized by APC's such as the ones shown in Figure 2b: I increases slowly over tens of angstroms sample displacement and always past the minimum of F. In this example, a compressive force of 2×10^{-7} N (solid arrow mark in the figure) was necessary to obtain a value of I of $\approx$1 nA on approach. The absolute value of F_m^i is found to vary between (1 and 3) $\times 10^{-7}$ N in these contacts. In contrast to type I contacts, the value of F_m^o is approximately equal to F_m^i, unless the maximum applied load F_M exceeds approximately 1×10^{-6} N.

3.1.2. Modulation Experiments: The Attractive Regime. The oscillation amplitude A, initially 9 Å peak-to-peak in the examples of Figure 2, decreases rather abruptly and is reduced to 50% of its initial value at 20–40 Å before the point of zero net force. This coincides with the onset of measurable attractive forces in the F curves in the top part of the figure. The rapid decrease of A at the point where F is still small indicates that weak perturbations of F result in a large decrease of A at resonance. The APC for A crosses the zero line due to a phase change of more than 90° and then reaches zero at around the minimum of F. Figure 4 gives additional details of the decrease of A in a type I contact. The top curve is the cantilever deflection with its superimposed oscillation (the frequency shown in the figure is lower than that of the actual lever oscillation due to the lower data collection frequency of about 1 kHz). The oscillation was not filtered out of the δ curve to better illustrate the change in oscillation amplitude as a function of distance and its decrease within the attractive part of F. We shall discuss this result in a later section.

3.1.3. Repulsive Force Regime. After the minimum in the F or δ is reached during approach of the sample, the direction of lever deflection changes sign and, after reaching zero, continues to increase monotonically with sample displacement. It should be noted that although upon crossing the x-axis, where $\delta = 0$, the force applied to the surface by the cantilever is zero, a compressive force is applied at the apex of the tip that is balanced by the long range attractive component of the van der Waals force acting on the volume of the tip, the capillary forces from fluids condensed around the tip apex area and short range adhesive forces across the tip–surface interface. The region of forces to the right of the minimum of the APC curves in Figures 2, 3, and 4 will be referred to as the repulsive force regime. In this regime the contribution of the attractive forces is mostly constant and approximately equal to the value of F at the minimum which is of the order of 1×10^{-7} N. The initial slope is less than unity (when measured in units of lever deflection) but approaches that value after several tens of angstroms. A slope of unity means that $\Delta d \approx \Delta\delta$, when the stiffness of the surface is much larger than the lever force constant. This initial curvature contains information about the elastic deformation of the substrate as we will discuss later.

The largest value of F is 3.4×10^{-6} N in Figure 2a and 1.3×10^{-6} N in Figure 2b and represents the maximum applied load F_M in these two cases. The total load is found by adding F_m^i to the force applied by the lever. When F_M is smaller than (1 to 2) $\times 10^{-6}$ N, we observed that the retract curve for F or δ (broken lines) closely overlaps the approach curve (continuous line), as shown in Figure 2b, due to elastic recovery. However, for larger values of F_M, the retract curves depart significantly from the approach ones, as can be seen in Figure 2a. As we shall discuss later, this is due to the plastic deformation of the gold substrate. Abrupt rupture of the contact with $F_m^o > F_m^i$ is observed in all type I contacts and in type II contacts when F_M is larger than (1 to 2) $\times 10^{-6}$ N. In the example of Figure 2a, the pull-off force F_m^o to break the contact is 4×10^{-7} N. This pull-off force was found to increase when F_M increased. As we shall discuss later, this is due to the formation of strong bonds between tip and surface as a

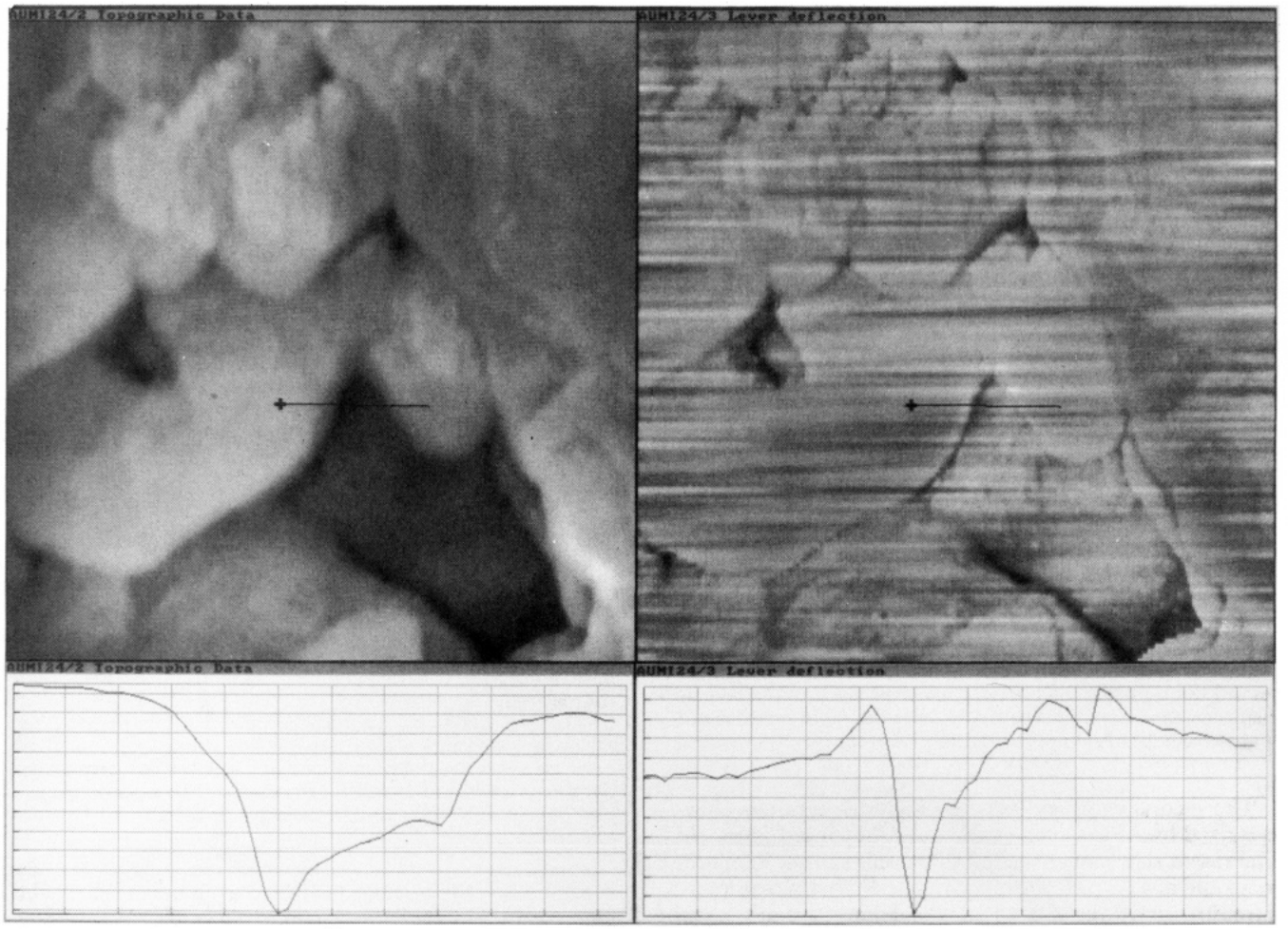

Figure 5. Top left: 5000 × 5000 Å STM image of the gold film at −0.1 V and 0.1 nA. Atomically flat terraces are observed with deep trenches between some of them. Top right: simultaneously measured dc lever deflection or force map. The horizontal streaks in this image are due to low frequency noise. The image is otherwise flat. Two profiles along the same line, as indicated in the two images are shown at the bottom. The horizontal divisions in both profiles are 100 Å and the vertical divisions are 5 Å for the STM topograph and 1 Å (corresponding to 3×10^{-8} N) for the lever deflection.

result of the disruption of passivating layers on the tip or on the surface.

3.2. Forces during STM Imaging in Air. Like other authors, we have imaged gold in air with conventional STM instruments. Monoatomic steps in Au(111) are observed with a height that corresponds to the expected interplanar spacing (≈2.3 Å) and atomic resolution can be obtained.[16] In view of the results presented in the previous sections, a question arises as to the forces acting during STM imaging in air. We begin by observing the hysteresis in the I APC's in Figures 2 and 3. In the case of type II contacts, current is not observed until a sufficiently large compressive force is reached during approach. We interpret this as due to the displacement of contaminats. Upon retraction the current persists down to the minimum of F, where the tip separates from the surface. In the case of type I contacts, current turns on quickly before contact. Past the minimum of F, metallic bonds form irreversibly and current persists until these bonds are broken upon retraction. The broken arrows in Figure 2 show the tip position for typical tunnel currents used in STM imaging. For type I contacts this position is to the left of the minimum, while for type II this may be on either side. Thus, the degree of contamination determines whether the force at the tip apex is repulsive during imaging.

Our combined AFM/STM can explore the spatial variation of the tip–surface force while the STM image is acquired. We show in Figure 5 a 5000 × 5000 Å image obtained by using the same tip as that used in the experiments of Figures 3 and 4. The left image is the topographic STM image taken at a 0.1 nA and 0.1 V bias (1 GΩ gap resistance). It shows several large grains (>1000 Å) that exhibit flat terraces, separated by trenches several tens of angstroms deep at the grain boundaries. The image on the right corresponds to the simultaneous dc lever deflection δ. (The horizontal stripes in the lever deflection image are artifacts due to low frequency noise.) The image is overall flat, i.e., constant lever deflection except at topographic depressions at the grain boundaries. There it shows a negative excursion that corresponds to an increase in the attractive force of less than 5×10^{-7} N. Since I is maintained constant by the feedback circuit, we can see that the profiles of constant force and constant current are not coincident. The increase in the attractive force in the depression over that in the flatter areas could be explained as a result of a larger effective curvature of the combined tip–surface system. This would increase the force due to both capilarity from weakly bound fluids and also from van der Waals interactions.

We have already shown the high sensitivity of the cantilever oscillation amplitude A to the presence of attractive forces. We imaged the area shown in Figure 5 a second time in the STM mode, but this time the ac

(16) Hallmark, V. M.; Chiang, S.; Rabolt, J. F.; Swalen, J. D.; Wilson, R. J. *Phys. Rev. Lett.* **1987**, *59*, 2879.

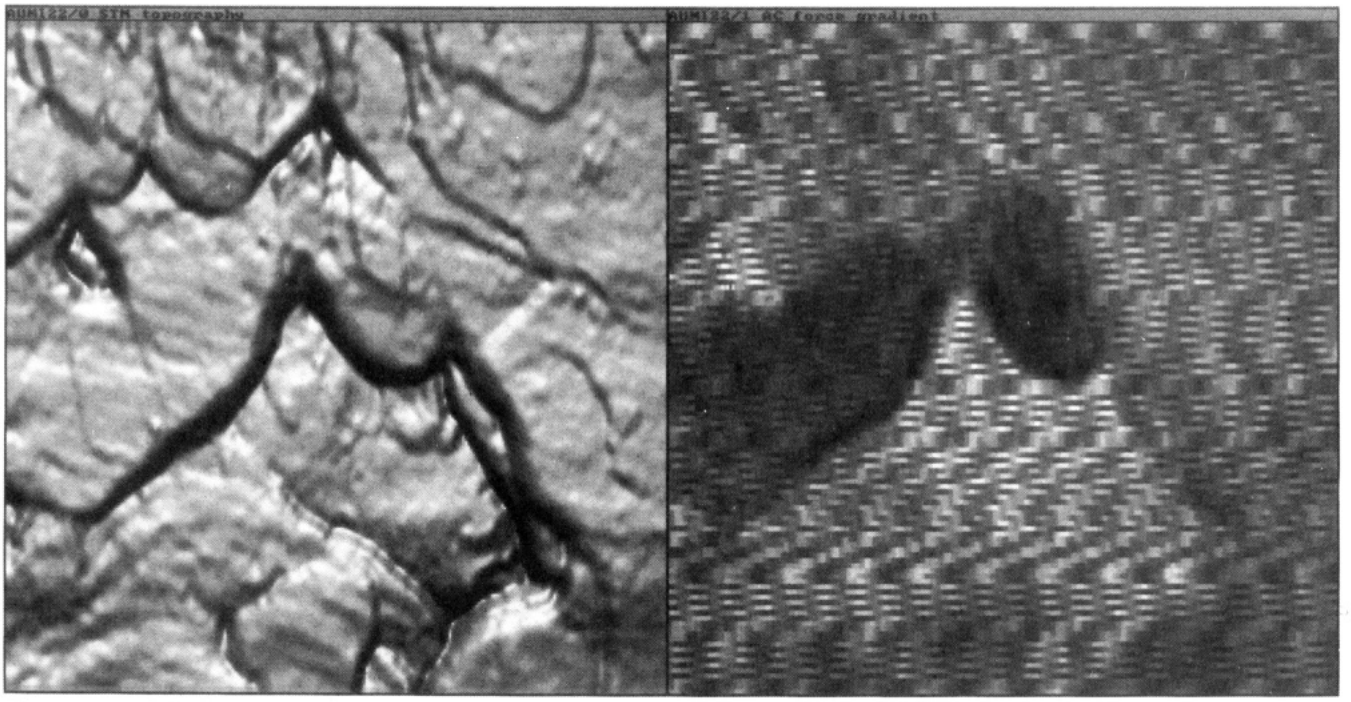

Figure 6. (a, left) STM image of the same region as in the image of the previous figure displayed in shaded form from an artificial light source to enhance contrast. (b, right) Simultaneously acquired in-phase oscillation amplitude A, showing a mostly flat surface except for the dark area in the center matches a topographic area in (a). The tip is in the attractive force region before the minimum of F. In the dark area the amplitude A is close to zero, probably due to a change in the sample contamination that is not detected in the dc F signal of the previous figure.

amplitude A was recorded simultaneously rather than the dc lever deflection. The STM topograph is shown in Figure 6a, which is almost identical to that of Figure 5a. The amplitude, A, produces the map shown in Figure 6b. The nonzero A signal indicates that, in this case, during STM imaging the tip is in the attractive region, to the left of the force minimum, as shown in Figure 4. As we can see, the image is essentially flat except for small contrast changes at the grain boundaries. An interesting difference is seen in the dark area near the center of the image which corresponds to a value of A near zero. This indicates that in this case the tip is at the minimum of F or in the repulsive region. This area is seen to correspond to certain grain boundaries in the STM image. This result could indicate a local change in composition or in the nature of the contaminants that is not detected in the STM topograph. It illustrates the usefulness of the ac mode of AFM imaging.

3.3. Plastic Deformation. The force required to plastically deform the substrate was determined by observing and measuring the marks left on the surface after applying forces F_M of increasingly larger values. Imaging was done in the STM or AFM ac mode. In the AFM attractive mode images of Figure 7 we show the result of a series of such experiments on gold films deposited on silicon. The top left image corresponds to the surface prior to the application of any force. We can observe several large grains that expose flat faces. The subsequent images in the same figure show the marks left after the application of the following forces: A for $F_M = 5 \times 10^{-6}$ N; B for $F_M = 3 \times 10^{-6}$ N; C for $F_M = 8 \times 10^{-7}$ N; D for $F_M = 3 \times 10^{-6}$ N; E again for $F_M = 3 \times 10^{-16}$ N. There is some variation in the size of the holes produced with a given force and in the threshold value of F that results in the production of a visible mark. The depth of the indentations is 100–200 Å for the larger values of F_M. For values of $F_M \leq 8 \times 10^{-7}$ N either no mark was observed or small (less than a few tens of angstroms) protrusions or holes were observed.

When clear indentation marks were observed, a "surface hardness" was calculated using the procedure of macroscopic hardness measurements (Vickers, Brinell, etc.[17]). The value of the applied load F_M is divided by the projected area of the observed indentation mark. The measurement of this area is not trivial as the shapes of the holes in the images are convolutions of tip and indentation shapes. The profile of a cut through a hole shows rounded edges such as those for hole D in Figure 7. If we assume that this curvature is due to the radius of the tip apex, this radius is then several hundred angstroms. Using this method, we obtained a value of the "surface hardness" for the (111) oriented gold film of 1 ± 0.5 GPa, close to the value reported by Guo et al.[18] and also to that obtained by Burnham et al.[5] of 0.65 GPa. The published value for the bulk hardness of gold is 0.5 GPa.[19] We shall comment further on this point in the discussion section.

Some of the work done on the sample during plastic deformation displaces material around the indentation. We noted that in general the amount of material seen around the indentation mark appears to be less than the volume of the indentation. It is not clear where the "missing" material went. Some of the material may be attached to the tip, and some may be accounted for by the production of numerous point defects such as interstitial gold atoms.[20] Work is also done in producing and moving dislocations. When dislocations emerge, they can produce step structures that were seen at times in the STM images. This is illustrated in the STM topographs of Figure 8,

(17) Blau, P. J.; Lawn, B. R. *Microindentation Techniques in Materials Science and Engineering*; American Society for Testing and Materials: Philadelphia, PA, 1985.

(18) Guo, Q.; Ross, J. D. J.; Pollock, H. M. *Mater. Res. Soc. Symp. Proc.* **1989**, *140*, 51.

(19) *Handbook of Tables for Applied Engineering Science*; The Chemical Rubber Co.: Cleveland, OH, 1970.

(20) Belak, J.; Stowers, I. F. Proceedings of the NATO ASI on Fundamentals of Friction; Braunlage/Harz, Germany, July 28–Aug 9, 1991.

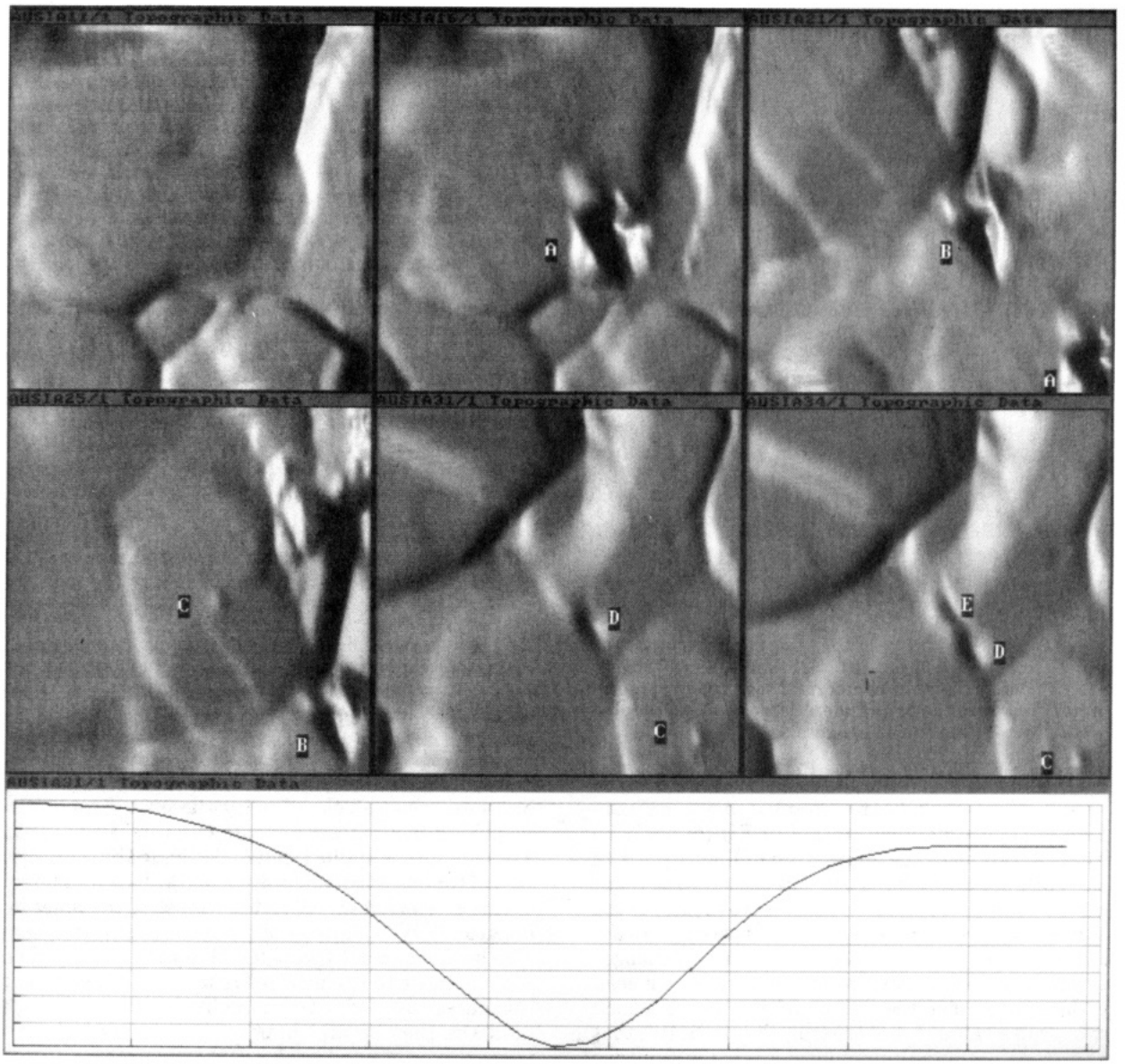

Figure 7. Indentation experiments to observe plastic deformation as a function of load. All 6000 × 6000 Å images were obtained in the ac AFM mode (attractive mode). At the top left we show the image prior to the application of any force. We can observe several large grains that expose the flat (111) face. The subsequent images show the holes, labeled A–E, produced after the application of the following forces: A, 5×10^{-6} N; B, 3×10^{-6} N; C, 8×10^{-7} N; D, 3×10^{-6} N; E, 3×10^{-6} N. The image frame was moved after each identation. The labels show equivalent points in the overlapping images. A profile across the shorter axis of identation mark D is shown at the bottom. Each horizontal division corresponds to 100 Å and each vertical division to 10 Å.

obtained at a gap resistance of 1 GΩ. Before the identation (a), the surface shows a number of curved monoatomic height steps in the upper half plus some other irregular features near the center. After an APC with F_M approximately 1×10^{-6} N applied near the bottom left edge, the STM reveals the formation of new steps. The indentation mark, was accompanied in this case by a "scratch" (bottom left) with displaced material at its edges. The scratch is due to a horizontal displacement of the sample during the approach in this experiment.

We summarize the observtions from a large number of experiments as follows:

(1) For $F < 1 \times 10^{-6}$ N, no indentation marks are observed except for occasional small bumps or holes observed sometimes, particularly for type I contacts, where forces in this range give rise to strong adhesive contacts, although the deformation is still mainly elastic.

(2) For $F > 1 \times 10^{-6}$ N substantial plastic flow of gold occurs. Some of the displaced material piles up around the indentation as shown in the images. Occasionally, dislocations are formed, visible at the surface as new steps.

4. Discussion

4.1. Types of Contacts: Contaminants. The variability in the values of F_m^i and in the onset point and rate of increase in the tunnel current indicates, not surprisingly, that contamination is present on the tip and surface in these air experiments to varying degrees. It is also experimentally observed, both by us and by many other authors, that STM images of Au(111) films in air show the atomic structure of this surface. Indeed, atomic resolution has been achieved in air when a number of chemically inert surfaces are imaged using a variety of different metal tips. Graphite is a common and well-known example. Metal surfaces covered by passivating adsorbates that form ordered monolayers have also been imaged with atomic

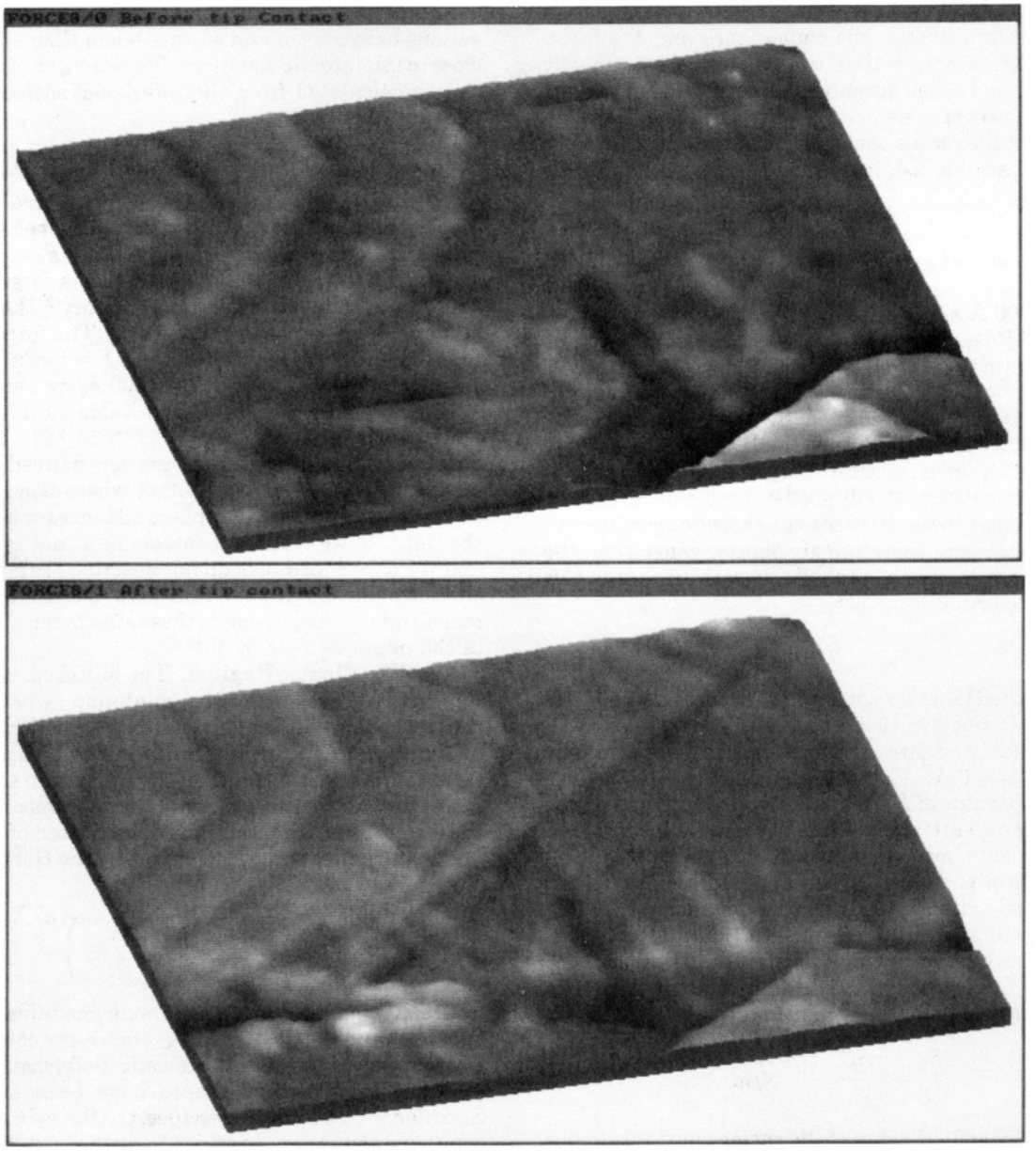

Figure 8. 3000 × 3000 Å STM images at −0.1 V bias and 0.1 nA current showing the gold substrate. Curved monoatomic steps are observed as well as other topographic features. Part a (top) is taken before the application of forces. Part b (bottom) is obtained after a load of approximately 1×10^{-6} N is applied. The contact point is at the bottom left, just outside the figure. Notice the new straight line step crossing diagonaly the image. Notice also the "scratch" near the bottom left that originates at the indentation mark just outside the figure.

resolution in air including S/Mo(001),[21,22] S/Re(0001),[23] and I/Pt(111).[24] These examples and our present results indicate that the layer of contaminants on the substrate in these cases consists most likely of weakly bound (physisorbed) layers of molecules, possibly water and hydrocarbons, that do not bind chemically to the surface and that are easily displaced by the tip. Their effect is mainly to exert capillary forces when the tip and surface films contact. From our F, δ, and A APC's we know that the total thickness of these films (substrate + tip) is typically 20–40 Å. We believe that in type I contacts *both* tip and substrate are mostly clean and are covered only by the weakly bound, easy to displace contaminants. In type II contacts, in contrast, additional strongly bound contaminants that cannot be easily displaced by the tip are present on either tip, substrate, or both. In a previous work,[25] we have shown that one monolayer of S chemisorbed on Re(0001) could prevent tip to surface adhesion in contacts where a total deformation of 20 Å in the surface and/or tip was produced. In the case of gold, the strongly bound layers are probably partially decomposed hydrocarbons.

4.2. Range and Origin of Forces. In order to facilitate the discussion of the previous experiments, we will review the types of forces that are likely to be present in our experiments and their order of magnitude.

Electrostatic forces arise when voltages are applied between the tip and surface and have the longest range. For a system formed by a semi-infinite flat substrate and

(21) Marchon, B.; Bernhardt, P.; Bussell, M. E.; Somorjai, G. A.; Salmeron, M.; Siekhaus, W. *Phys. Rev. Lett.* **1988**, *60*, 1166.
(22) Marchon, B.; Ogletree, D. F.; Bussell, M. E.; Somorjai, G. A.; Salmeron, M.; Siekhaus, W. *J. Microsc.* **1989**, *152*, 427.
(23) Ogletree, D. F.; Ocal, C.; Marchon, B.; Somorjai, G. A.; Salmeron, M. *J. Vac. Sci. Technol.* **1990**, *A8*, 297.
(24) Schardt, B. C.; Yau, Shueu-Lin; Rinaldi, F. *Science* **1989**, *243*, 1050.
(25) Salmeron, M.; Ogletree, D. F.; Ocal, C.; Wang, H.-C.; Neubauer, G.; Kolbe, W. *J. Vac. Sci. Technol.* **1991**, *B9*, 1347.

a spherical tip, the method of image charges can be used to calculate numerically the capacitance and the force. The calculation shows that the capacitance is mostly determined by the background shape and size of the tip. The force however is determined by the shape of the tip apex. When the radius of curvature of the apex region R, is greater than the distance to the sample s, the force is approximated by

$$F_e \simeq \frac{3RV^2}{s} \times 10^{-11}\ \mathrm{N} \quad (1)$$

For R = 1000 Å and s = 100 Å, $F \approx (3 \times 10^{-10})V^2$ (V in volts). For V less than a few volts, F_e is negligible in the scale of Figure 2. We have detected electrostatic forces by applying voltages of a few volts. They were found to be of long range as predicted by the above formula. However, since at present only small bias voltages were applied (<1 V), electrostatic forces played a negligible role in our experiments and will not be discussed further.

van der Waals forces between the extended surface and tip decay as s^{-2} and therefore are shorter range than the electrostatic ones. For a parabolic tip with an apex radius R, the nonretarded force is[26]

$$F_w = -HR/6s^2 \quad (2)$$

where H is the Hamaker constant. For metals like Au, $H \approx 4 \times 10^{-19}$ J. For R = 1000 Å, in direct contact ($s \approx 3$ Å), $F_w \approx 8 \times 10^{-8}$ N, and through an interposed layer of atomic adsorbates ($s \approx 6$ Å), $F_w \approx 2 \times 10^{-8}$ N. These values are similar to the value of F_m^i in many of our contacts. At the range where the attractive force becomes measurable in our experiments however, about 30 Å, $F_w \approx 8 \times 10^{-10}$ N, which is below the noise level. Thus, forces other than van der Waals are operating at this distance.

The tip will snap into the surface (jump to contact), whenever the cantilever force constant k is less than the tip–surface force gradient. By differentiating the above expression for F_w, one finds that for R = 1000 Å

$$\frac{\partial F_w}{\partial s} = \frac{HR}{3s^3} \approx \frac{10^4}{s^3}\ \mathrm{N/m} \quad (3)$$

with s in Å. Since the value of the spring constants of our cantilevers is usually in the 100's of N/m, van der Waals forces will not cause a jump of the tip of more than 4–5 Å. This is the reason that stiff cantilevers must be used for these studies.

Capillary forces are exerted when fluid films are present like the layers of contaminants. The capillary force is given by

$$F_c = 4\pi R\tau \cos\theta \quad (4)$$

where τ is the surface tension of the fluid and θ the contact angle. For an order of magnitude estimate we can take $\theta \approx 0$. For water, for example, τ = 73 mJ/m^2, so that for R = 1000 Å, $F_c = 1 \times 10^{-7}$ N. For many hydrocarbons (alkanes, benzene) $\tau \approx$ 20–25 mJ/m^2, giving $F_c = 3 \times 10^{-8}$ N. These values are the same order of magnitude as the observed attractive forces in our experiments. Moreover, since contaminant layers may have a thickness of a few tens of angstroms, their presence is the most likely cause of the attractive force observed that is felt at distances ranging from 20 to 40 Å away from the point of zero net force. Only near contact are van der Waals and capillary forces comparable in our case.

(26) For a review see, for example Israelachvili, J. N. In *Intermolecular and Surface Forces*; Academic Press: London, 1985.

Short range adhesive forces arise from bonding interactions between tip and surface when their separation is close to interatomic distances. The strength of these forces can be calculated from the interfacial surface energy w per unit area by

$$F = \partial \pi r_0^2 w/\partial h \quad (5)$$

where r_0 is the radius of the contact area and h the displacement of the applied load. For a spherical tip of radius R reversibly deforming a flat, $F = 2\pi Rw$. An accurate treatment of the contact area is given by the Johnson–Kendall–Roberts (JKR) theory,[27] that takes into account the increase in r_0 due to w. The force necessary to break the contact is found to be $F = 3\pi Rw$. With $w \approx$ 2 J/m^2 (for clean Au) and R = 1000 Å, we obtain $F = 1.5 \times 10^{-6}$ N, and for $w \approx 0.1$ J/m^2, a value more appropriate for Au in air,[18] we obtain $F = 7.5 \times 10^{-8}$ N. We want to emphasize that these equations are derived on the assumption of a reversible contact where bonds form and break continuously as the sphere advances or recedes from the flat. As we will see, contacts need not be reversible and the above formulas do not describe the pull-off force correctly, although they still give the correct order of magnitude. A discussion of these effects can also be found in the paper by Guo et al.[18]

4.3. The Elastic Regime. The initial curvature of the force curves just after the minimum, when repulsive contact begins, can be explained by the elastic deformation of the tip and substrate. Since in the present case the substrate is much softer than the tip, we can assume than in the first approximation only the substrate deforms. In the elastic approximation, the deformation of the surface under an applied force F_{def} is given by the Hertz formula[28]

$$F_{def} = \frac{4R^{1/2}}{3\left(\frac{1-\nu_{Au}^2}{E_{Au}} + \frac{1-\nu_{Pt}^2}{E_{Pt}}\right)} h^{3/2} \quad (6)$$

where E_{Au} and E_{Pt} are the Young modulus of the Au substrate and the Pt–Rh tip, ν_{Au} and ν_{Pt} the corresponding Poisson ratios, and h the elastic deformation. Other relations for different shapes have been analyzed by Sneddon.[29] Two limiting shapes, the flat cylinder and the cone, give power dependencies on h of 1 and 2, respectively. The force F_{def} in eq 6 is the net compressive force $F_M + F_m^i$ since, as we mentioned, the attractive force is compensated by an equal and opposite repulsive force at zero external load. To obtain h, we simply subtract the cantilever deflection $\Delta\delta$ from the sample displacement Δd measured from the minimum of the δ APC. A plot of $\Delta\delta$ vs Δd for the data of Figure 2b is shown in Figure 9. The continuous lines represent the behavior expected from the equation shown above using the macroscopically determined elastic parameters of gold. As reported also by Cohen et al.,[6] at small deformations the effective radius of the tip, 500 Å in this case, is smaller than the average radius of 1000 Å determined by SEM. This can be explained by the existence of a small protrusion at the apex that determines the contact at low loads, while at larger loads it is the average radius that is important due to the deformation of the small apex protrusion. A similar plot for the data of Figure 2a can be fitted by a radius of ≈4000 Å, which is somewhat larger than the average macroscopic radius.

(27) Johnson, K. L.; Kendall, K.; Roberts, A. D. *Proc. R. Soc. London* 1971, *A324*, 301.

(28) Timoshenko, S. P.; Goodier, J. N. *Theory of Elasticity*; McGraw-Hill Publishing Co.: New York, 1970.

(29) Sneddon, I. N. *Int. J. Eng. Sci.* 1965, *3*, 47.

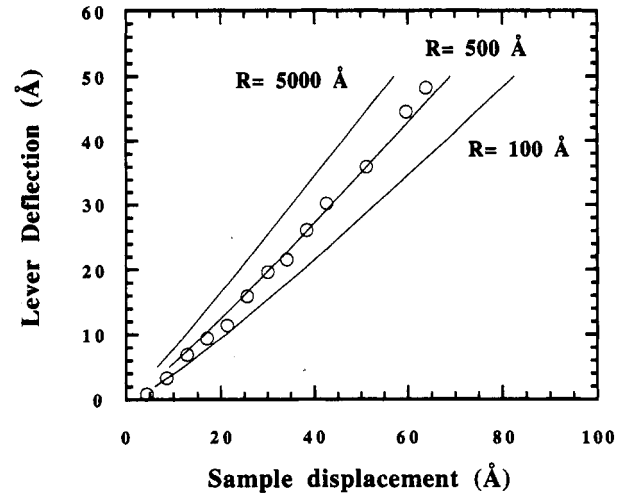

Figure 9. Lever deflection, $\Delta\delta$, versus sample displacement, Δd, measured from the minimum of the APC in Figure 2b. This region is expanded here to show the curvature that is particularly visible at the start of the compressive force regime. The curvature is due to the elastic deformation of the gold substrate. Three curves that represent the behavior expected from purely elastic theory (equation 6 in the text) for three different radii are shown. The points deviate from the line corresponding to a 500-Å tip radius above Δd = 50 Å, when the deformation $\Delta d - \Delta\delta$ is 14 Å.

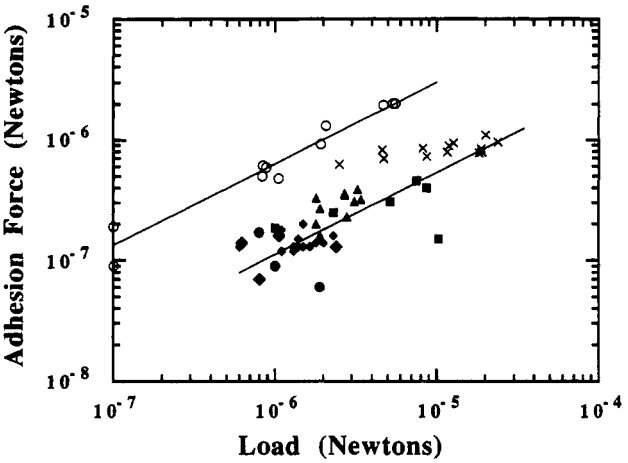

Figure 10. log–log plot of the adhesion force F_{adh} measured as the difference between the pull-off force to break contact during retraction F_m^o and the attractive force F_m^i, versus maximum applied load F_M. Each set of filled symbols correspond to the same tip at different points of the sample. The cross symbols are at a point where a high degree of contamination was present. The open symbols at the top represent a different set of experiments immediately after preparing a new fresh tip. The lines drawn through each set of points have a slope of 2/3.

4.4. Metallic Adhesion. As mentioned in the Experimental Section, the pull-off force to break the contact on retraction, F_m^o, is always larger than the attractive force minimum observed during approach F_m^i for type I contacts. This is true even when the net applied force is negative, as shown in Figure 3. For type II contacts, this effect is only observed for loads F_M larger than (1 or 2) × 10^{-6} N. This is due to the formation of metallic bonds between tip and substrate atoms. The adhesion force due to these bonds, F_{adh}, can be obtained as being approximately equal to $F_m^o - F_m^i$, since the capillary and van der Waals attraction contributions are present during both approach and retraction.

A log–log plot of F_{adh} versus load, $F_M + F_m^i$, is shown in Figure 10 for both types of contacts. The filled symbols represent different series of APC's for type II contacts. Each series is obtained with the same tip but at different locations on the surface. One of these regions (cross symbols) was unusually contaminated to the extent that the tunnel current I did not start until a repulsive force of more than 5 × 10^{-6} N was applied. The open circles correspond to experiments performed immediately after etching a new fresh tip that produced contacts of type I. Two lines have been drawn in this figure with slope 2/3 as a visual aid.

We can explain the observed variation of F_{adh} with load by assuming that once metallic bonds form between tip and surface during loading, they do not break during unload until the minimum of F is reached, i.e., the contact is irreversible. Strong metallic bonds form from the start of the repulsive regime for type I contacts. As the load increases, the area of contact and also the number of metallic bonds formed increases. This accounts for the observed increase of F_{adh}. When strongly bound contaminants are present (type II contacts), bonds will form only after the application of forces large enough to displace the contaminant layers.

To explain the functional dependence of F_{adh} on load, we will assume first that the elastic regime applies and that the area of contact can be calculated from the Hertzian model. If r_0 is the radius of the contact area, the adhesion force will be that necessary to break $\pi r_0^2/\sigma$ bonds (σ = area per atom). The Hertzian contact radius r_0 is given by[28]

$$r_0^3 = \frac{3}{4} FR\left(\frac{1-\nu_{Au}^2}{E_{Au}} + \frac{1-\nu_{Pt}^2}{E_{Pt}}\right) \qquad (7)$$

Since we propose F_{adh} to be proportional to r_0^2, a 2/3 power dependence on the load should exist. The slope of 2/3 in Figure 10 agrees with the predictions of eq 7. The scattering of the data in the figure, particularly for the experiments on type II contacts, could be due to the variation of the average bond energy across the contact in different indentations, due to residual contaminants not displaced during loading. Equation 7 can be modified to include the increase in contact area due to the bonds formed at the interface as is done in the Johnson–Kendall–Roberts (JKR) theory.[27] The correction however is only important at loads below approximately 1 × 10^{-7} N and therefore unimportant in our case.

Since indentation marks are observed when the load is above 10^{-6} N, it is clear that plastic deformation occurs under the contact area and that in the load range of Figure 10 the transition from elastic to fully plastic behavior takes place. In the fully plastic regime, the area of contact should be simply proportional to the load and produce a slope of 1 in Figure 10. The agreement of the results with the slope of 2/3 indicates that elastic deformations are still dominant and that full plasticity is not reached until the highest loads.

We can also compare the radius of the contact area r_0, predicted by the elastic and fully plastic models. For a tip radius of 1000 Å, eq 7 predicts $r_0 \approx 100$ Å for a load of 10^{-6} N and $r_0 \approx 225$ Å for a load of 1 × 10^{-5} N. When corrected for the interface adhesion as in the JKR theory, the values are 120 and 235 Å, respectively (assuming $w \approx 0.1$ J/m^2). These predicted values are about a factor of 2 smaller than the average radius of the indentation marks produced by these two loads ($r_0 \approx$ 180 and 565 Å, respectively). We shall discuss this point further in the next section.

Let us discuss now the magnitude of the force to break metallic bonds, F_b, that is found from these experiments. As an example we can take the point where the adhesion force F_{adh} = 6 × 10^{-7} N in the open circles series of Figure

10 that corresponds to a load 1×10^{-6} N. By dividing F_{adh} by the number of atoms in the contact area (assuming 7.2 Å^2 per atom as in Au(111)), we obtain $F_b \approx 1.3 \times 10^{-10}$ N for $r_0 = 100$ Å. We can make a simple estimate of the force to break a metal bond by considering a bond length increase of 1 Å as leading to rupture. For a bond energy of ≈1 eV, $F_b \approx 1$ eV/1 Å $= 1.6 \times 10^{-9}$ N. The lower value of F_b found in our experiments can be explained by assuming that only a fraction of the atoms in the contact area form metallic bonds due to residual impurities and imperfect lattice mismatch between the tip and substrate interfaces.

The data points shown as crosses in Figure 10 are fit with a slope approaching zero, consistent with contamination mediated contacts that prevent formation of metallic bonds. As will be discussed in a later paper, this behavior is also found in gold films with adsorbed layers of alkanethiols.[30]

4.5. Plastic Deformation. We initiate the discussion by estimating the load under which the elastic limit of gold is exceeded (F_{lim}). This occurs when the pressure exerted by the load F (which can be calculated using eq 7) equals (within 10%) the yield stress of gold (about 1 GPa). The result is $F_{lim} \approx 4 \times 10^{-8}$ N for a 1000 Å radius tip. This value is reached right after the minimum of F, often in the attractive force regime when the load is still negative. According to classical contact mechanics,[28] the point where the plastic deformation is initiated is located at a depth of $0.5r_o$ below the contact center (about 15 Å in our case). However, as discussed in the classical book of Bowden and Tabor,[8] outside this point the deformation is still essentially elastic. Full plasticity is reached at a higher load, F_{plas}, when the pressure increases to about 2.8 times the yield pressure of gold. Using the same values as before, this gives $F_{plas} = 1 \times 10^{-6}$ N, at which point the plastically deformed region reaches the surface. These figures agree roughly with our observations of plastic behavior that are summarized in section 3.3. If a similar calculation is performed for the Pt–Rh 13% tip, we found $F_{lim} \approx 1 \times 10^{-5}$ N and $F_{plas} \approx 2 \times 10^{-4}$ N, which indicates that no plastic deformations of the tip occur in our experiments.

Another possibility that we have not discussed so far is that part of the identation mark is due to material removed by the tip and attached to it during rupture of the metallic adhesion, in addition to the displaced material from the purely plastic deformation. A better measurement of hardness would be obtained by preventing metallic adhesion. This could be achieved by interposing strongly bound monolayers of passivating atoms, as we reported for S adsorbed on Re(0001).[24] The relatively large error bar of ±0.5 GPa found in our hardness measurements might be partially due to the variation in hole size depending on the adhesion of material onto the tip.

The measured value of 1 GPa for the hardness of Au(111) films is similar to the macroscopic value of 0.5 GPa, that is obtained in experiments involving a much greater volume of gold in the indentation process. Using gold foils and applying loads in the range of μN, Burnham and Colton,[5] found a hardness value of 0.65 GPa, not far from our measured value. Pethica et al.[31] found, for work-hardened polycrystalline gold, an increase in the value of the hardness from around 0.5 GPa when the indentation depth is in the micrometer range up to 2 GPa when the indentation size decreased to 300 Å. This scale dependence of the hardness has been explained either by extreme local work hardening[31] of the gold substrate or by the absence of dislocations.[32] Our gold films on silicon substrates are composed of flat single crystal grains that are several thousand angstroms in a diameter, a factor of 5 larger than the indentation marks. In the case of mica substrates, the grains were larger. We observed no difference in the hardness for these two substrates. The hardness was also independent of load and depth of indentation within our experimental error.

5. Summary and Conclusions

Our observations on the interaction between single asperity Pt–13% Rh alloy tips and a Au(111) films can be summarized as follows:

a. In air environments, the attractive interaction before contact is dominated by capillary forces due to layers of contaminants. These forces became measurable at distances between 20 and 40 Å before contact, both in the dc mode and more clearly when monitoring the modulation amplitude of the cantilever. The combined van der Waals and capillary forces have a maximum strength in the range of 1×10^{-8} to $(1–2) \times 10^{-7}$ N.

b. Compressive forces result in the elastic deformation of the gold substrate until a critical load of approximately 1×10^{-6} N is reached (for our average apex radius of around 1000 Å). Above this load the Au(111) film substrate yields plastically leaving a permanent indentation mark, occasionally with steps that can be observed with STM. The hardness value obtained from these experiments is 1 ± 0.5 GPa.

c. Metallic adhesion between tip and substrate occurs in clean contacts for all loads and for contaminated contacts when the load is above (1 or 2) $\times 10^{-6}$ N. The force necessary to break the metallic bonds between tip and substrate varies as the $^2/_3$ power of the load and is due to the corresponding increase in contact area.

d. In air, tunnel current between the Pt–Rh tip and the gold substrate can be observed either before or after the minimum of the interaction force is encountered, depending on the degree and nature of the contamination.

Acknowledgment. This work was supported by the Lawrence Berkeley Laboratory through the Director, Office of Energy Research, Basic Energy Science, Materials Division, of the US Department of Energy under Contract Number DE-AC03-76SF00098. Additional support was also provided by a grant from the DOW Chemical Company.

(30) Salmeron, M.; Neubauer, G.; Folch, A.; Kolbe, W.; Ogletree, F. To be submitted for publication.

(31) Pethica, J. B.; Hutchings, R.; Oliver, W. C. *Philos. Mag. A* **1983**, *48*, 593.

(32) See, for example, Hull, D.; Bacon, D. J. In *Introduction to Dislocations*; Pergamon Press: Oxford, 1984.